J. Comp. App. Res. Mech. Eng. Vol. 12. No. 2, pp. 247-261, 2023 *DOI: 10.22061/JCARME.2022.8347.2124*

Journal of Computational and Applied Research in Mechanical Engineering
jcarme.sru.ac.ir
SRTTU
JCARME
ISSN: 2228-7922

Research paper

Unsteady state numerical study of carbon deposition on the performance of solid oxide fuel cell and variation of porosity

H. Khoshkam[a], K. Atashkari[a,*] and M. Borji[b]

[a] *Department of Mechanical Engineering, University of Guilan, P.O. Box 3756, Rasht, Iran*
[b] *Department of Mechanical Engineering, Lahijan Branch, Islamic Azad University, Lahijan, Iran*

Article info:

Article history:

Received: 23/08/2021
Revised: 26/09/2022
Accepted: 28/09/2022
Online: 01/10/2022

Keywords:

Solid Oxide Fuel Cell,
Carbon deposition,
Porosity change,
Numerical simulation,
Temperature distribution,

[*]Corresponding author:
atashkar@guilan.ac.ir

Abstract

Carbon deposition has a serious effect on the failure mechanism of solid oxide fuel cells. A comprehensive investigation based on a two-dimensional model of a solid oxide fuel cell with the detailed electrochemical model is presented to study the mechanism and effects of carbon deposition and unsteady state porosity variation. Studies of this kind can be an aid to identify the SOFC optimal working conditions and provide an approximate fuel cell lifetime. It has been revealed that, due to carbon deposition, the porosity coefficient of the fuel cell decreases. Consequently, a reduction in the amount of fuel consumption along the fuel cell and the chemical and electrochemical reaction rates are resulted which can be clearly seen in the off-gases molar ratio. The percentage of output fuel changes in the timeframe is useful information for optimizing CHP systems including fuel cells. The percentage of the output water vapor, which usually increases compared to the input, decreases by 17% at the end of the working period. Also, unreacted methane in the output of the fuel cell increased by 12%; in other words, it is wasted. The other consequence of carbon deposition reduced electrochemical and chemical reaction rates and the reduction of temperature difference along the cell. The study shows that after 145 working days, the temperature difference along the cell varies from 117 °C for the starting time to 7 °C. Also, by reducing the current density, the cell output power density decreases by 72% after 145 working days.

1. Introduction

Solid oxide fuel cells (SOFCs) are considered a technology for the combined generation of electrical and thermal energy. Early fuel cells were designed to use hydrogen because it is easy to convert electrochemically and, when hydrogen is used as fuel, there is only water as a product [1, 2]. The major advantages of solid oxide fuel cell systems are potential for direct use of hydrocarbon fuels and the use of renewable energy, which makes fuel cells an important source of energy for the future [3-5]. SOFCs have been investigated numerically and less experimentally from different points of view, such as; SOFC-only or SOFC-based combined heat and power (CHP) system optimization, the parametric study in various operating conditions such as shape, temperature, pressure, and flow direction [6-9]. Numerical

solution has found a special place due to the high cost and difficulty of laboratory solutions [10, 11]. The fuel and air channels in the fuel cell can be considered co-flow, counter-flow, and cross-flow. In two-dimension solid oxide fuel cells analysis, the counter flow configuration has been shown to be more efficient than co-flow, but both the temperature gradient and the maximum temperature inside the cell are higher. It is expected that without careful consideration, this large temperature gradient will lead to cell destruction [1, 12]. The main parts of the fuel cell are the anode, electrolyte, and cathode which is called PEN (Positive electrode /Electrolyte /Negative electrode) structure. Since performance improvement has always been a major aim for designing fuel cells, the study of PEN structure has received much attention [13-17].

Regardless of the fuel used in a SOFC, a complex collection of different phenomena momentum, energy, and mass transport along with chemical and electrochemical reactions, occur inside the flow channels, porous electrodes, and solid electrolyte [18, 19]. The fact that different kinds of fuels, like; hydrogen, syngas, and hydrocarbons can be used in the SOFC, frequently has been asserted in the literature. But, when using a hydrocarbon fuel, despite many advantages, the problem of carbon deposition cannot be ignored [20, 21]. Reduced porosity, ion permeability, catalyst activity, and as a result reduced electric efficiency and finally, SOFC degradation are the consequences of carbon deposition. According to thermodynamic analysis, an increase in the ratio of steam to carbon (S/C) or temperature changes, is proposed to prevent carbon deposition, but unfortunately, the thermodynamic analysis is not appropriate in this case because it assumes that the rates of the forward reaction (carbon deposition) and the reverse reaction (carbon removal) are rapid enough to establish equilibrium, an assumption that cannot be justified [22]. Mostafaeipour *et al.* [23] presented the ANFIS method to select highly influential parameters for the proton exchange membrane (PEM) element of fuel cells. Yan *et al.* [24] developed a numerical model, with the operating temperature at 800 °C, to predict carbon deposition molar mass. The anodic porosity and the electrical conductivity that are affected by carbon deposition are taken into account. The unsteady relation between the changes in H_2O/CH_4 ratio and carbon deposition was determined. The results showed that the changes in the anode porosity in time-dependent solution can lead to a 7 % reduction in the fuel cell's electrical efficiency. Xu *et al.* [25] presented the lattice Boltzmann model (LB) to investigate the local distributions of deposited carbon in the porous anode of methane feed solid oxide fuel cell. The results showed the severe effect of heterogeneity of anode microstructure and the operating temperature on carbon deposition. Ma *et al.* [26] selected a two - dimensional model to perform a study on carbon deposition phenomena in SOFC. They concluded that the increase in the molar fraction of hydrogen, pressure, and temperature will increase the amount of carbon content. The deposition of carbon in the anode porous media for two different types of carbon in thermodynamic equilibrium conditions was done by Schluckner *et al.* [27]. Using a new approach for modeling, they studied the amount of carbon deposition in different conditions and different fuel ratios and components. As mentioned, the factors affecting the carbon deposition rate have been examined in several studies, but still, there are unclear aspects of this phenomenon and its effects on the system [28].

Reducing entropy loss has always been the challenge of different power and heat production systems and various methods have been used to optimize it [29].

Since the complexity of solving problems in fuel cells is high, the Lattice-Boltzmann model can be a suitable option for estimating parameters and heat flow and transfer [30]. In addition, new approaches have been implemented in the field of combining fuel cells with other renewable energies such as solar energy to reduce air pollution and increase the performance of fuel cell-based systems [31, 32].

In the present study, a complete numerical method is used in seven separate sections, namely the air and fuel flow channels, the cathode and anode support and catalyst layers, and the electrolyte. The time-dependent governing equations with suitable boundary conditions are solved by the use of COMSOL Multiphasic commercial software. All-important electrochemical and chemical reactions such as methane cracking reaction

(MCR), water-gas shift reaction (WGSR), Boudouard reaction (BR), methane steam reforming reaction (MSRR) and CO and H_2 oxidation are solved in a specified layer simultaneously affected by other layers. Time-dependent carbon deposition and its effect on the anode porosity, different reaction rates inside the anode porous media, cell temperature distribution, SOFC efficiency, and economic considerations, are the main goal of the study.

2. Physical models and computational method

A schematic diagram of an anode-supported co-flow planar type:
A cell consisting of air and fuel flow channels, anode and cathode support (diffusion) and reaction (catalyst) layers, and electrolyte is presented in Fig. 1. Syngas fuel which is composed of CH_4, CO, H_2, CO_2 and H_2O flows thorough the fuel channel and air, mainly consisting of N_2 and O_2 enters the air channel. As illustrated in Fig. 1, four main reactions, namely WGSR, MSRR, MCR and BR, take place inside the anode support or diffusion layer while CO and H_2 are electrochemically oxidized inside the anode reaction or catalyst layer. A detailed unsteady two-dimensional model is used to analyze time- dependent carbon deposition and porosity variation and thereby electric performance of SOFC in a 150-day working period. The composition of fuel enters the anode channel and other SOFC main geometrical and operating conditions are given in Table 1.
Four dominant chemical reactions and two electrochemical reactions considered in the present model are as follows;

$$CH_4 + H_2O \leftrightarrows 3H_2 + CO \quad \text{(MSRR)}$$

$$CO + H_2 \Leftrightarrow C + H_2O \quad \text{(BR)}$$

$$CO + H_2O \Leftrightarrow CO_2 + H_2O \quad \text{(WGSR)}$$

$$CH_4 \Leftrightarrow C + 2H_2 \quad \text{(MCR)}$$

$$H_2 + \frac{1}{2}O_2 \rightarrow H_2O$$

$$CO + \frac{1}{2}O_2 \rightarrow CO_2 \quad \text{Electrochemical reactions}$$

$$H_2 + O^{2-} \rightarrow H_2O + 2e^- \quad \text{Anode}$$

$$CO + O^{2-} \rightarrow CO_2 + 2e^- \quad \text{Anode}$$

$$0{,}5O_2 + 2e^- \rightarrow O^{2-} \quad \text{cathode}$$

2.1. Electrochemical model and conservation of electronic and ionic charge

As it is shown in Fig. 1, cell electrochemical reactions will be occurred in the most active area of the electrodes namely, anode and cathode catalyst or reaction layer near the electrodes triple phase boundaries (TPBs) [33].
In many studies, the relationship between activation polarization and electric current density has been calculated by the Butler-Volmer equation Eq. (1) [10].

$$j = j_0 \left\{ \exp\left(\frac{\alpha \eta_{act\,i} n_e F}{RT}\right) - \exp\left(\frac{-(1-\alpha)\eta_{act\,i} n_e F}{RT}\right) \right\} \quad (1)$$

The rate of electrochemically oxidation of hydrogen and carbon monoxide, and reduction of oxygen can be written by use of Faraday's law Eqs. (2-4):

$$\dot{r}_{elec\,H_2} = \dot{r}_{elec\,H_2O} = \frac{j_{H_2}}{2F} \quad (2)$$

$$\dot{r}_{elc\,CO} = \dot{r}_{elec\,CO_2} = \frac{j_{CO}}{2F} \quad (3)$$

$$\dot{r}_{elec\,O_2} = \frac{j_{O_2}}{4F} \quad (4)$$

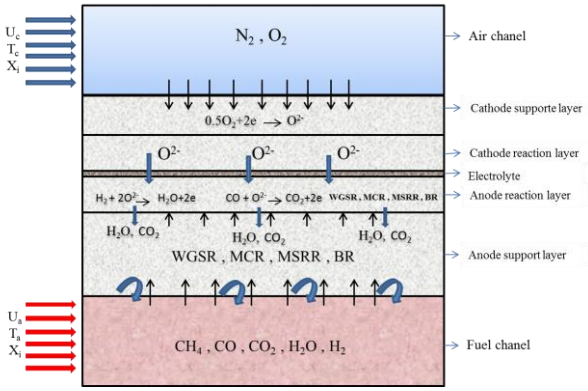

Fig. 1. Schematic of planar SOFC model.

Table 1. Physical dimension and working parameters of the model [15, 25].

Working temperature	1073 K
Length of the cell	0.1 m
Initial porosity of anode	0.4
Porosity of cathode	0.4
Working pressure	1 atm
Height of the fuel channel	1×10^{-3} m
Height of air channel	1×10^{-3} m
Cathode supported layer thickness	2.5×10^{-5} m
Anode supported layer thickness	4×10^{-4} m
Thickness of electrolyte	8×10^{-6} m
Cathode reaction layer thickness	1.3×10^{-3} m
Anode reaction layer thickness	2×10^{-3} m
Inlet molar fraction of N_2	% 0.79
Inlet molar fraction of O_2	% 0.21
Inlet molar fraction of H_2	% 0.044
Inlet molar fraction of CO	% 0.493
Inlet molar fraction of CO_2	% 0.029
Inlet molar fraction of CH_4	% 0.263
Inlet molar fraction of H_2O	% 0.171
Aperture of cathode supported layer	1.4×10^{-6} m
Aperture of anode supported layer	2×10^{-6} m
Tortuosity of electrode	4.5
Faraday's constant	96487 C mol^{-1}
Inlet velocity	1.2 m s^{-1}

The reversible electrical potential of a cell, or open circuit potential, is a local parameter that depends on the local temperature, and the composition of the gas mixture as a fuel. Considering H_2 and CO electrochemical reactions, this parameter can be calculated based on Nernst equation as follows [34, 35]:

$$E^{rev}_{H_2-O_2} = E^0_{H_2-O_2} - \frac{R_u T}{2F}\ln\left[\frac{P^{fc}_{H_2O}}{P^{fc}_{H_2},(\frac{P^{ac}_{O_2}}{100000})^{0,5}}\right] \quad (5)$$

$$E^{rev}_{CO-O_2} = E^0_{CO-O_2} - \frac{R_u T}{2F}\ln\left[\frac{P^{fc}_{CO_2}}{P^{fc}_{CO},(\frac{P^{ac}_{O_2}}{100000})^{0,5}}\right] \quad (6)$$

In these correlations E^0 represents open-circuit potential at the standard temperature and pressure and unity activity, and is the function of Gibbs free energy change for electrochemical reactions Eqs. (7, 8):

$$E^0_{H_2-O_2} = -\frac{\Delta G^0}{2F} = -\frac{g^0_{H_2O} - {}^1\!/_2\, g^0_{O_2} - g^0_{H_2}}{2F} \quad (7)$$

$$E^0_{CO-O_2} = -\frac{\Delta G^0}{2F} = -\frac{g^0_{CO_2} - {}^1\!/_2\, g^0_{O_2} - g^0_{CO}}{2F} \quad (8)$$

If an electrical current is drawn from a fuel cell, the voltage reduces in response to five loss mechanisms of a cell. The mechanisms are electrode activation, and concentration over potentials and internal resistances.

$$E_{cell} = E^{rev}_{H_2-O_2} - (\eta_{conc\,O_2} + \eta_{act\,O_2}) - (\eta_{conc\,H_2} + \eta_{act\,H_2}) - \eta_{Ohm} \quad (9)$$

$$E_{cell} = E^{rev}_{CO-O_2} - (\eta_{conc\,O_2} + \eta_{act\,O_2}) - (\eta_{conc\,CO} + \eta_{act\,CO}) - \eta_{Ohm} \quad (10)$$

According to iterative procedure proposed by Iwai *et al.* [35], the ratio of J_{H2} and J_{CO} is determined so that the potentials obtained for parallel part of Fig. 2 match each other.

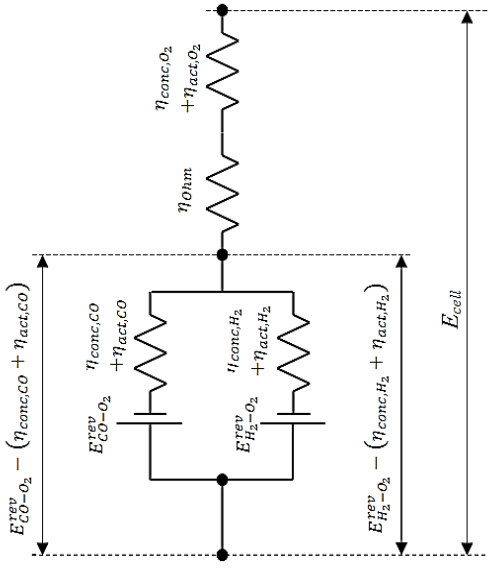

Fig. 2. Equivalent circuit model for current and voltage calculations.

The conservation of electronic and ionic charge in the interconnect layer can be calculated as:

$\nabla, j_l = 0$ Conservation of ionic charge

$\nabla, j_s = 0$ Conservation of electronic charge

Where (j) is the current density and it is described by Ohm's law as Eq. (11):

$$j_l = -\sigma_l \nabla \varphi_{el} \quad (11)$$

$$j_s = -\sigma_s \nabla \varphi_{i0} \quad (12)$$

where σ is the electronic or ionic conductivity and $\nabla\phi$ is the electronic or ionic potential, respectively.

2.2. Conservation of momentum

The velocity of the fluid flow in the cathodic and anodic channels along with porous electrodes affects the rate of heat transfer in the cell and plays an important role in controlling the cell operating temperature. Furthermore, the effect of chemical reaction rates influenced by temperature field on the electric performance of the cell cannot be ignored. Despite of the fact that at high electric currents or low voltages, the models considering momentum equation give more accurate results [36], many studies do not take it into account.
In this study, well-known Navier-stokes equation has been used to calculate the variation of velocity and pressure inside the flow channels Eq. (13) [24]:

$$\rho \frac{\partial u}{\partial t} - \nabla, [\eta(\nabla u + (\nabla u)^T)] + \rho(u, \nabla)u + \nabla p = s \quad (13)$$

While the Brinkman equation is employed as the momentum conservation equation in the porous media Eq. (14) [25]:

$$\frac{\rho}{\varepsilon}\frac{\partial u}{\partial t} + \left(\frac{\eta}{k} + \mathrm{S}\right)\mathrm{u} = \nabla, \left[\frac{\eta}{\varepsilon}(\nabla u + (\nabla u)^T)\right] - \nabla p \quad (14)$$

In this equation η stands for the dynamic viscosity and S introduces the momentum source terms for each calculation domain, namely; anode support and reaction layer (ASL, and ARL), cathode reaction layer (CRL) and fuel flow channel which are listed in Eqs. (15-18) [24].

$$S_{ASL}=R_{msrr}(M_{CO}+3M_{H2}-M_{CH4}-M_{H2O})+R_{wgsr}(M_{CO2}+M_{H2}-M_{CO}-M_{H2O})+R_{mcr}(2M_{H2}-M_{CH4})+R_{BR}(M_{CO2}-2M_{CO}) \quad (15)$$

$$S_{fuel} = R_{wgsr}(M_{CO2}+M_{H2}-M_{CO}-M_{H2O}) \quad (16)$$

$$S_{CRL} = \frac{-JM_{O2}}{4F} \quad (17)$$

$$S_{ARL} = R_{msrr}(M_{CO}+3M_{H2}-M_{CH4}-M_{H2O}) + R_{wgsr}(M_{CO2}+M_{H2}-M_{CO}-M_{H2O}) + R_{mcr}(2M_{H2}-M_{CH4}) + R_{BR}(M_{CO2}-2M_{CO}) + \frac{J(M_{H2O}-M_{H2})}{2F} + \frac{J(M_{CO2}-M_{CO})}{2F} \quad (18)$$

The parameters R_{msrr}, R_{wgsr}, R_{mcr}, and R_{BR} are the rate of MSRR, WGSR, MCR, and BR, respectively. These parameters can be defined mathematically as Eqs. (19-22);

$$R_{msrr} = a(K_{f\,msr}P_{CH_4}P_{H_2O} - K_{b\,msr}P_{CO}P_{H_2}) \quad (19)$$

$$R_{wgsr} = a(K_{f\,wgsr}P_{CO}P_{H_2O} - K_{b\,wgsr}P_{CO_2}P_{H_2}) \quad (20)$$

$$R_{mcr}= a\left(\frac{1}{3600M_c}\frac{K_{f\,mcr}(P_{CH_4}-P_{H_2}^2/K_{p\,mcr})}{(1+K_{H_2}\sqrt{P_{H_2}})^2}\right) \quad (21)$$

$$R_{BR}= a\left(\frac{1}{3600M_c}\frac{K_{CO}K_{f\,B}(P_{CO}-\frac{P_{CO_2}}{P_{CO}K_{p\,B}})}{(1+K_{CO}P_{CO}+\frac{P_{CO_2}}{P_{CO}K_{CO}P_{CO}})^2}\right) \quad (22)$$

Above mentioned correlations for the rate of four dominant chemical reactions will be used to calculate the sink or source terms for each gaseous specious inside the cell.

2.3. Mass transfer equation

Considering the multi-component fluid flow and the porous structure of the electrode, three mass transfer mechanisms, namely viscous flow, bulk diffusion and diffusion, into the porous medium are involved. As mentioned earlier a syngas consisting of methane, hydrogen, carbon monoxide, carbon dioxide, and water vapor is supplied to the fuel channel. On the other side, a binary mixture of oxygen and nitrogen enters the air channel.
The unsteady state specious mass conservation equations have been stated as follows in Eq. (23):

$$\rho\frac{\partial\omega_i}{\partial t}+\nabla,j_i+\rho(u,\nabla)\omega_i=S_i \quad (23)$$

In this equation, parameters u, ω_i, j_i and S_i stands for Velocity field, mass fractions and source term. The relation between current density, mass fraction of each specious and moles of transferred electrons can be written as Eq. (24) [24];

$$N_i=j_i+\rho u\omega_i \quad (24)$$

in which, j_i and related parameters are as Eqs. (25-27);

$$j_i=-(\rho\omega_i\sum D_{ik}d_k+D_i^T\frac{\nabla T}{T}) \quad (25)$$

$$d_k=\nabla x_k+\frac{1}{P_A}[(x_k-W_k)\nabla P_A \quad (26)$$

$$x_k=\frac{\omega_k}{M_k}M_n \quad , \quad M_n=(\sum\frac{\omega_i}{M_i})^{-1} \quad (27)$$

The bulk diffusion coefficient can be calculated by the use of Fuller equation and a multi-component approach Eq. (28) [3];

$$D_{b,i}= \frac{1-X_i^{fc}}{\sum_{j\neq i}\frac{X_i^{fc}\cdot\frac{P^{fc}}{10^5}\left[\frac{2}{M_i^{-1}+M_j^{-1}}\right]^{0.5}\cdot\left[V_{dif,i}^{1/3}+V_{dif,j}^{1/3}\right]^2}{1.43\times10^{-7}T_{fc}^{1.75}}} \quad (28)$$

With following definition for i and j;

i	j			
H_2	H_2O	CH_4	CO	CO_2
H_2O	H_2	CH_4	CO	CO_2
CO	H_2O	H_2	CH_4	CO_2
CO_2	H_2O	H_2	CH_4	CO

Finally, the Knudsen diffusion coefficient has been expressed as Eq. (29) [3];

$$D_{K\,i}=\frac{2}{3}r_P\sqrt{\frac{8RT}{\pi M_i}} \quad (29)$$

The source terms of Eq. (23) are related to reactions in which each specious participates which are listed in Table 2.

2.4. Energy conservation

Considering the high operating temperature of the SOFC, two heat transfer mechanisms, namely, heat conduction and convection have been taken into account. Also, as it is precedent [16], local thermal equilibrium between solid and fluid inside the porous electrodes can be assumed.

Table 2. Mass transfer source terms in each layer.

Fuel channel	$S_{H_2} = R_{wgsr}M_{H_2}, S_{H_2O} = -R_{wgsr}M_{H_2O}, S_{CH_4} = 0, S_{CO} = -R_{wgsr}M_{CO}, S_{CO_2} = R_{wgsr}M_{CO_2}$
Anode support layer	$S_{H_2} = \left(R_{wgsr} + 3R_{msrr} + 2R_{mcr} - \frac{J}{2F}\right) * M_{H_2}$
Anode support layer	$S_{H_2O} = -\left(R_{wgsr} + R_{msrr} + \frac{J}{2F}\right) M_{H_2O}$
	$S_{CH_4} = -(R_{wgsr} + R_{mcr})M_{CH_4}, S_{CO} = \left(R_{msrr} - R_{wgsr} - 2R_B - \frac{J}{2F}\right) M_{CO},$
	$S_{CO_2} = \left(R_{wgsr} + 2R_B + \frac{J}{2F}\right) M_{CO_2}$
Anode reaction layer	$S_{H_2} = (R_{wgsr} + 3R_{msrr} + 2R_{mcr})M_{H_2}, S_{H_2O} = -(R_{wgsr} + R_{msrr})M_{H_2O},$
	$S_{CH_4} = -(R_{wgsr} + R_{mcr})M_{CH_4}, S_{CO}, = (R_{msrr} - R_{wgsr} - 2R_B)M_{CO}$
	$S_{CO_2} = (R_{wgsr} + 2R_B)M_{CO_2}$
Cathode reaction layer	$S_{O_2} = \frac{-JM_{O2}}{4F}$

It is worth noting that, because of zero gas velocity, only heat conduction within the electrolyte and interconnector is considered Eq. (30):

$$(\rho C_p)^{eff}\frac{\partial T}{\partial t} + \rho C_{p\,gas}\mathrm{u}, \nabla, T - \nabla, K^{eff}\nabla, T = Q \quad (30)$$

where k^{eff} and C_P^{eff} are the effective thermal conductivity and specific heat at constant pressure, $C_{P,\,gas}$ is the gas mixture specific heat at constant pressure and Q is the heat source or sink Eqs. (31, 32) [33]:

$$K^{eff} = \varepsilon K_{gas} + (1-\varepsilon)K_{solid} \quad (31)$$

$$C_p^{eff} = \varepsilon C_{p,gas} + (1-\varepsilon)C_{P,solid} \quad (32)$$

As mentioned, different chemical and electrochemical reactions occur within the SOFC which can play the role of heat sources or sinks in the energy equation. Heat is generated by the enthalpy change due to the electrochemical reaction, the ohmic, concentration and activation polarizations within the PEN structure as well as by the water-gas shift, Boudouard reactions occurring in the anode and fuel channel. On the other hand, heat is consumed by the internal steam reforming reactions within the anode and the change of entropy in the anodic electrochemical reactions [15, 37].

2.5. Unsteady carbon deposition model

Two main reactions which are involved in the process of carbon deposition, namely, Boudouard and methane cracking reactions, occur within the anode diffusion and reaction layers that are assumed to be continued. Deposited carbon covers the anode surface and reduces the reactions of the active surface area, changes the porosity coefficient of the anode and hence, and reduces the catalyst activity expressed by following reactions [24, 32];
The carbon deposition rate r_C is Eqs. (33-35):

$$r_c = \frac{dC_c}{dt} = a(\mathrm{R}_{mcr} + R_{Br}) \quad (33)$$

$$\frac{d\alpha}{dt} = -K_a r_c^2 C_c \alpha \quad (34)$$

$$\frac{\mathrm{d}\varepsilon}{\mathrm{dt}} = \frac{dV_c}{dt}\frac{1}{V_{tot}} = \frac{\varepsilon r_c M_c}{\rho_c} \quad (35)$$

The variation of anode porosity would influence the permeability in porous layer Eq. (36):

$$K = K_0 \left(\frac{\varepsilon}{\varepsilon_0}\right)^{3.55} \quad (36)$$

Fuel cell operating conditions affect the amount of carbon deposition and consequently changes the microstructures of porous surfaces. For example local velocity, temperature, gaseous specious mole fraction, pressure, local chemical and electrochemical reactions affect the rate of carbon deposition locally.

2.6. Boundary conditions

Considering the mathematical nature of each unsteady conservation equation, initial values and proper boundary conditions must be taken into account. The cell operating voltage is implemented at the lower boundary of anode support layer and the interface of electrode reaction layers and electrolyte is assumed to be continuous. Velocity inlet boundary condition has been chosen at the entrance of flow channels while pressure outlet is specified at the outlet. For the specious mass conservation equation, the mole fractions of each gaseous specious are assigned. In order to solve the energy conservation equation, the inlet temperature is implemented.

3. Validation

In order to verify the results of the present study, one experimental report and two numerical solutions have been used. The comparison of the current model with the experimental data and numerical results of Martin Anderson *et al.* [38] regarding the current density, cell voltage and Power density have been illustrated in Fig. 3. As it can be seen, results are in sufficiently reasonable agreement with the literatures.
Furthermore, the results of Yan *et al.* [24] have been used to validate the model performance in carbon deposition simulation. As it can be seen from Fig. 4, the proposed model fully responded to the desired conditions with high accuracy.

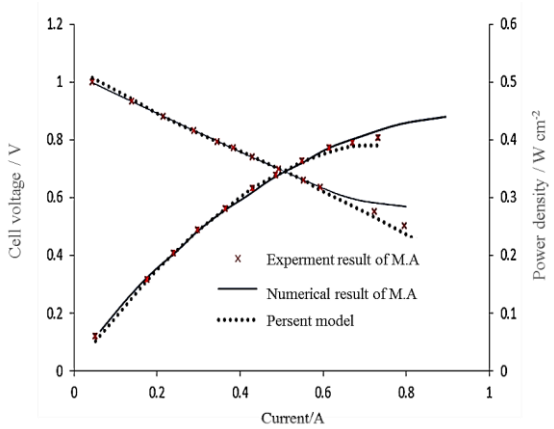

Fig. 3. Comparisons between the measured and model predicted performance.

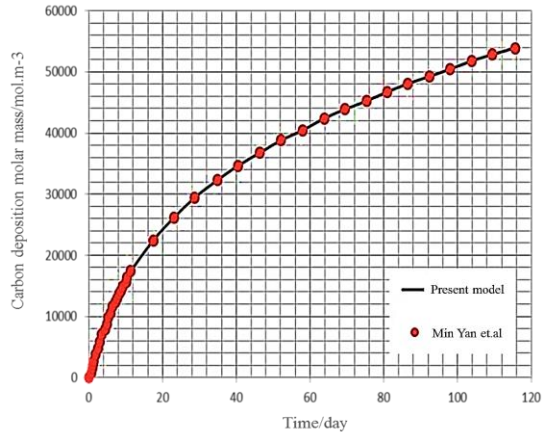

Fig. 4. Validation of carbon deposition.

4. Results and discussion

The time-dependent carbon deposition at 1073 ˚K is shown in Fig. 5 The precipitated carbon is formed due to two dominant reactions namely Baudouard and methane cracking reactions.
As it is shown, the rate of carbon deposition process for the first 20 days, is higher than those of the next 130 days. This fact can be deduced from the slope of the curve of these two periods. As it is reported earlier, carbon deposition will reduce the porosity and disrupts the catalyst performance as depicted in Fig. 6. Therefore, over time, the deposition rate decreases significantly. The results show that the porosity coefficient decreases by 37% after carbon deposition during 150 working days.

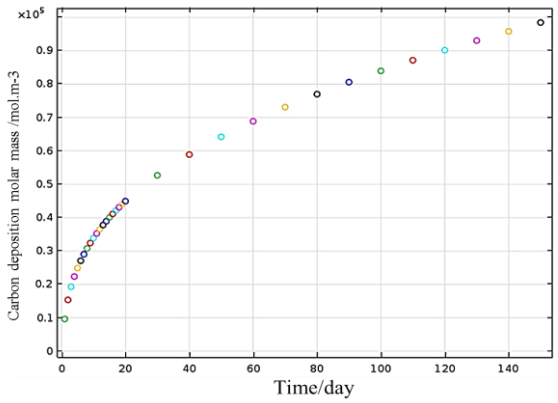

Fig. 5. Carbon deposition molar mass.

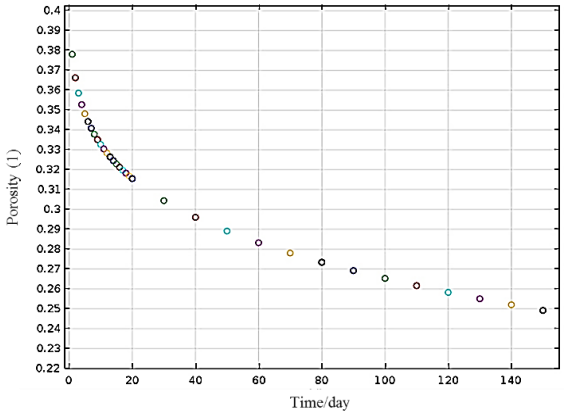

Fig. 6. Porosity change over time.

4.1. Heat transfer

Temperature profile is an influential and important factor in the destruction mechanism of the fuel cell. The endothermic reactions like MSR and the exothermic reactions like WGSR and electrochemical reactions, form the temperature profile in the fuel cell. Without considering the effect of carbon deposition, the temperature profile is governed by the flow characteristics and electrochemical reactions as well as electrical resistance. These factors lead to an increase in initial temperature of the fuel cell at the inlet up to 1180 ˚K at the outlet of the cell (Fig. 7). Carbon deposition reduces the rate of the reactions, and also the electrochemical reaction hence as depicted in Fig. 8, the temperature rise decreases after 60 working days. This phenomena is clearer after 145 working days as illustrated in Fig. 9. But as can be seen, the temperature profile decreases first and then increases due to carbon deposition along the fuel cell. The main reason for this is the reduction of the electrochemical reactions and the heat produced due to electrical resistance. Therefore, MSR is the determinant reaction of temperature profiles so the temperature drops. Methane content decreases rapidly accordingly and tends to zero in the middle of the cell, so the result changes to the exothermic reactions and the temperature rises again.

Fig. 10 shows the temperature gradients along the cell length for the first, 30, 60 and 145 working days. The figure illustrates that the output temperature decreases by 50 ˚C (4.6%) after 30 days, by 70 ˚C (6%) after 60 days and by 120 ˚C (10%) on the 145th day. As it can be seen, the temperature decreases by 4.6% during the first 30 days, by 1.4% in the second 30 days, and by only about 4% in the next 85 days, which indicates a decrease in the sedimentation rate.

4.2. Power density

As discussed, carbon deposition reduces the rate of electrochemical reactions via decreased porosity and catalyst activity. Electric performance of the cell regarding cell power density is shown in Fig. 11. The maximum power of 0.36 W/cm^3 decreased by 33% after 25 days, and on the 60th day this reduction reaches 44% and its value becomes 0.2 W/cm^3.

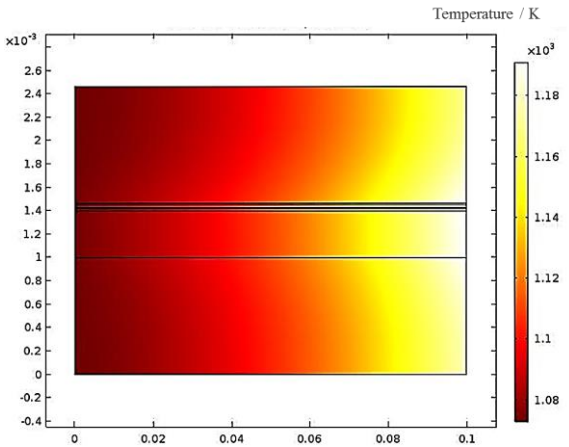

Fig. 7. Temperature distribution before carbon deposition.

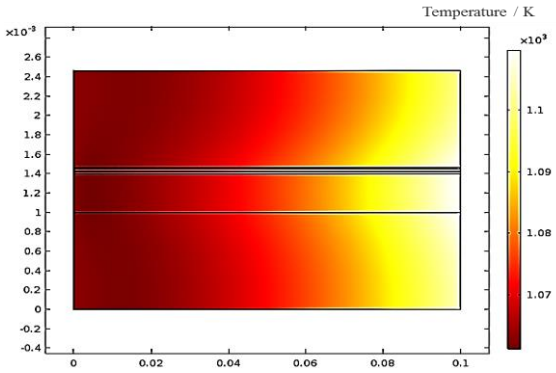

Fig. 8. Temperature profile after 60 working days.

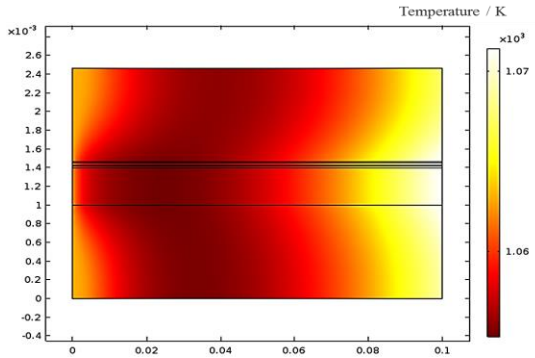

Fig. 9. Temperature profile after 145 working days.

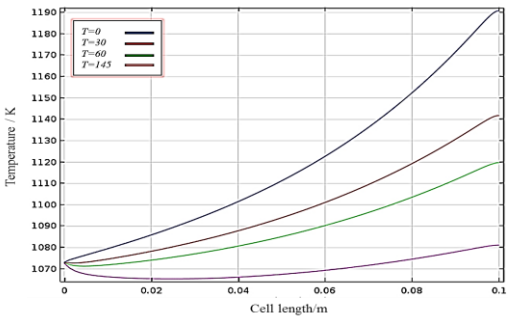

Fig. 10. Temperature distribution in the longitudinal direction of the fuel cell at times 0, 30, 60 and 145 day of working.

The power reduction will drop below 0.1 W/cm^3 and will change by 72% on the 145th day. Due to the physical changes caused by carbon deposition such as the reduction of the porosity and permeability coefficient, the performance of the fuel cell has decreased significantly. Therefore, carbon deposition will greatly affect the useful life of the fuel cell.

4.3 output component change after carbon deposition

Carbone deposition leads to decreased porosity coefficient which in turn entails the reduction in the effective diffusion coefficient of each gaseous specious within the porous electrodes.
Fig. 12 shows the mole fraction of gas specious along the cell length without considering the effect of carbon deposition.
Aftter carbon deposited, the rate of chemical and electrochemical reactions will be changed and the mole fractions of specious can be affected.
On the other side, reduced operating temperature which is one of the main consequences of carbon deposition plays an important role in controlling the reaction rates. The amount of change in fuel cell performance can be estimated by determining the changes in the mole fraction of the output components.
Fig. 13(a) shows the percentage of changes in H_2 after 150 working days in fuel channel output relative to inlet fuel.

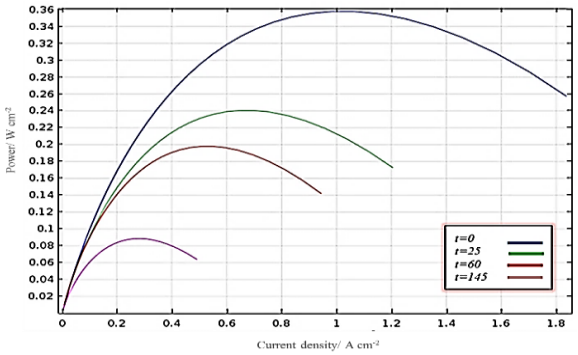

Fig. 11. Variation of cell performance at different time.

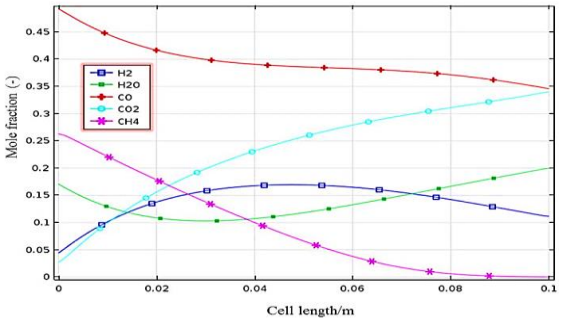

Fig. 12. Changes in the amount of gas components along the fuel cell.

It can be seen that H_2 increases by 45% in outlet of fuel channel after 30 working days; this increases to 64% in 60 days, 75% in 90 days, and 95% in 150 days. A closer look at the mechanism of H_2 variation reveals that H_2 produces by three main chemical reactions namely, WGSR, MCR and MSRR, and consumed by the electrochemical reaction of hydrogen. Initially, due to the high reaction rate of WGSR and MCR, the H_2 mole fraction increases and gradually by increasing the rate of the electrochemical reaction, depletion will occurred. But H_2O which is produced by electrochemical reaction and consumed by WGSR, and MSRR varies in reverse.

As it can be deduced from Fig. 13(b), H_2O was produced by 15.3% before carbon deposition and showed an increase compared to input H_2O. After carbon deposition, the percent change of H_2O on day 60 reaches almost zero and on day 150, it decreases by 12% compared to the initial state. Therefore, carbon deposition reduces the rate of water production reactions and increases the rate of water consumption reactions.

The CO and CO_2 mole fractions at the outlet of fuel channel have been shown in Fig. 13(c) and Fig. 13(d).

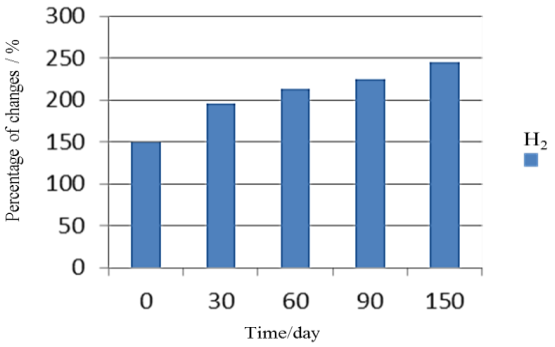

(a)

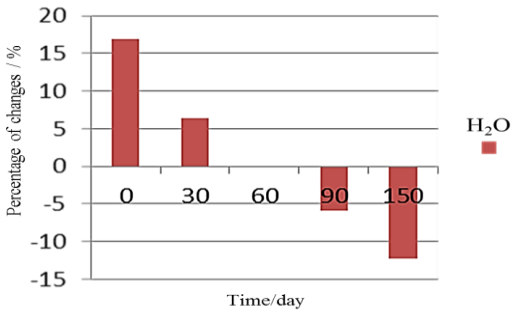

(b)

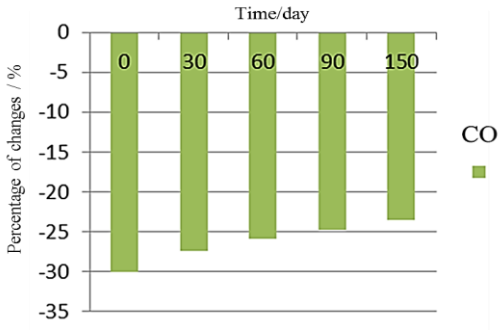

(c)

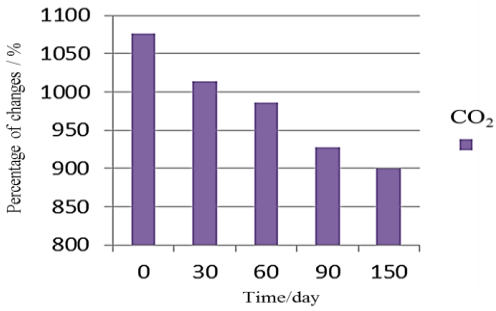

(d)

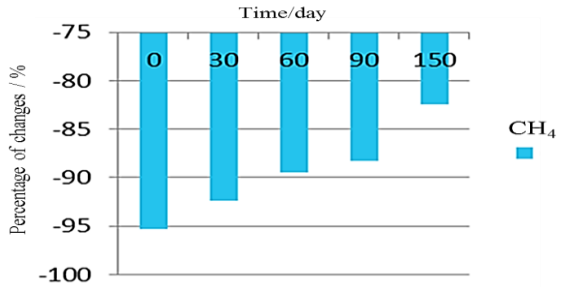

(e)

Fig. 13. Percentage of changes in components after 150 working days in fuel channel output relative to inlet fuel (a) for H_2, (b) for H_2O, (c) for CO, (d) for CO_2, and (e) for CH_4 .

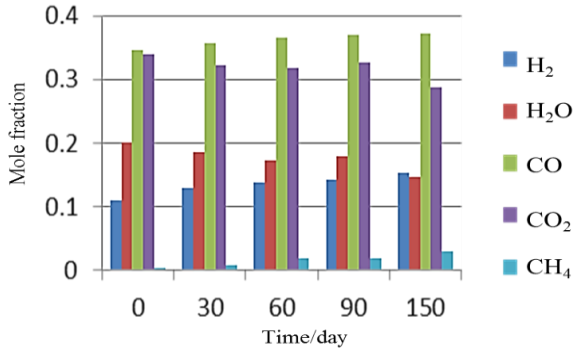

Fig. 14. Mole fraction changes after 150 working days in fuel channel output.

The CO and CO_2 mole fractions at the outlet of fuel channel have been shown in Fig. 13(c) and Fig. 13(d). CO is produced by MSRR and consumed via BR, WGSR and the electrochemical reaction. Overly, the rate of the consumption is dominant and CO mole fraction decreases along the cell. But the decrease in the amount of the CO at the outlet of the fuel channel reduces by 3, 4, 5 and 6 at 30, 60, 90 and 150 working days, respectively. On the other side, CO_2 is produced by WGSR and the electrochemical reaction of *CO*, hence the CO_2 mole fraction increases from 0.029 at the inlet to 0.341 at the outlet of fuel channel (about 1076%) as depicted in Fig. 13(d). It is worth to note that considering the effect of carbon deposition, CO_2 mole fraction at the outlet of fuel channel decreases about 62, 90, 148 and 176 after 30, 60, 90 and 150 working days, respectively. At the entrance of the fuel channel, methane is consumed by high rate MCR and MSRR and there is no methane content in the mixture at the outlet of the fuel channel. Furthermore, at the mentioned times, the changes in the output methane will be 3%, 6%, 7% and 13%, respectively, compared to the non-deposition state (Fig. 13(e)). As a summary, as it is clear from Fig. 14, the mole fraction H_2O and CO_2 decrease by carbon deposition and the mole fraction CH_4, H_2 and CO increase after carbon deposition.

5. Conclusions

Unsteady state behavior of a direct internal reforming SOFC considering the effect of carbon deposition has been numerically investigated in two dimensions. Time-dependent variation of porosity and catalyst activity has been modeled and verified against the available experimental and numerical studies. The SOFC main parameters, such as electric performance, two-dimensional temperature distribution, gaseous specious mole fraction with and without carbon deposition consideration have been analyzed to clarify the effect of deposited carbon on the performance of the cell. The porosity coefficient and carbon deposition were investigated.

The results showed that during 150 working days, the porosity coefficient decreases by 37% due to the effect of covering the porous surface with carbon and these changes are noticeably visible in the first 20 working days. The physical changes made in the fuel cell due to carbon deposition cause changes in the system operation. The results also show that the temperature profile is strongly affected by carbon deposition and the temperature gradient changes drastically, which is an important factor in fuel cell degradation.

Maximum temperature at the outlet of the channels has decreased about 10% at the end of the working period. Changes in the percentage of the output fuel components is one of the very interesting and important results obtained. It is shown that, considering carbon deposition after 150 working days, there is about 7% more CO gas in the exhaust gas than in the initial state. As the results showed, almost 95% methane consumed at the beginning of the fuel cell due to the rapid reaction of the methane cracking reaction, but after carbon deposition, the unconsumed methane in the exhaust gas is about 12% more.

It has been concluded that the reduced porosity and catalyst activity can severely decrease the cell power density (about 72%). The information provided is very important and useful for performance optimization, active control of the CHP systems including fuel cells, design and structure improvement of fuel cell systems.

References

[1] M. Andersson, J. Yuan and B. Sundén, "Line approach and simulation for anode–supported SOFC", *ASME 7th international "fuel cell science, Engineering and Technology Conference"*, California, USA, pp. 539-549, (2009).

[2] Y. Patcharavorachot, A. Arpornwichanop and A. Chuachuebsuk, "Electrochemical study of a planar solid oxide fuel cell: Role of support structures", *J. Power Sour.*, Vol. 177, No. 2, pp. 254-261, (2008).

[3] M. Borji, K. Atashkari, S. Ghorbani and N. Nariman-Zadeh, "Model-based evaluation of an integrated autothermal biomass gasification and solid oxide fuel cell combined heat and power system", *J. Mech. Eng. Sci*., Vol. 231, No. 4, pp. 31251–3140, (2015).

[4] N. L. Panwar, R. Kothari and V. V. Tyagi, "Thermo chemical conversion of biomass e eco-friendly energy routes", *Renew. Sustain. Energy. Rev*., Vol. 16, No. 4, pp.1801-1816, (2012).

[5] R. Toonssen, S. Sollai, PV. Aravind, N. Woudstra and AHM. Verkooijen, "Alternative system designs of biomass gasification SOFC/GT hybrid systems", *Int. J. Hydrogen. Energy.*, Vol. 36, No. 16, pp. 10414-25, (2011).

[6] H. Xu and Z. Dang, "Numerical investigation of coupled mass transport and electrochemical reactions in porous SOFC anode microstructure", *Int. J. Heat. Mass. Transfer*., Vol. 109, pp. 1252–126, (2017).

[7] M. Borji, K. Atashkari, S. Ghorbani and N. Nariman-Zadeh, "Parametric analysis and Pareto optimization of an integrated auto thermal biomass gasification, solid oxide fuel cell and micro gas turbine CHP system", *Int. J. Hydrogen Energy*, Vol. 40, No. 41, pp. 14202-14223, (2015).

[8] M. C. Williams, J. P. Strakey, W. A. Surdoval and L. C. Wilson, "Solid oxide fuel cell technology development in the U.S", *Solid State Ionics*, Vol. 177, No. 19-25, pp. 2039-2044, (2006).

[9] I. Khazaee and A. Rava, "Numerical simulation of the performance of solid oxide fuel cell with different flow channel geometries", *Energy*, Vol. 119, pp. 235-244, (2017).

[10] J. Alinejad and J. A. Esfahani, "Numerical Stabilization of Three-Dimensional Turbulent Natural Convection Around Isothermal Cylinder", *J. Thermophys. Heat. Transfer.*, Vol. 30, No. 1, pp. 94-102, (2016).

[11] S.M. Madani, J. Alinejad, Y. Rostamiyan and K. Fallah, "Numerical study of geometric parameters effects on the suspended solid particles in the oil transmission pipelines", *J. Mech. Eng. Sci*., Vol. 236, No. 8, pp. 3960-3973. (2021).

[12] M. Fardadi, D. F. McLarty and F. Jabbari, "Investigation of thermal control for different SOFC flow geometries", *Appl. Energy*, Vol. 178, pp. 43–55, (2016).

[13] M. Borji, K. Atashkari, N. Nariman-zadeh and M. Masoumpour, "Modeling, parametric analysis and optimization of an anode-supported planar solid oxide fuel cell", *J. Mech. Eng. Sci*, Vol. 229, No. 17, pp. 1–16, (2015).

[14] T. Meng, D. Cui, Y. Ji, M. Cheng, B. Tu and Z. Lan, "Optimization and efficiency analysis of methanol SOFC-PEMFC hybrid system", *Int. J. Hydrogen. Energy.*, Vol. 47, No. 64, pp. 27690-27702, (2022).

[15] M. Andersson, J. Yuan and B. Sundén, "Review on modeling development for multiscale chemical reactions coupled transport phenomena in solid oxide fuel cells", *Appl. Energy*, Vol. 87, No. 5, pp. 1461–1476, (2010).

[16] O. Razbani and M. Assadi, "Artificial neural network model of a short stack solid oxide fuel cell based on experimental data", *J. Power Sour. Adv.*, Vol. 246, pp. 581-586, (2014).

[17] M. Tafazoli1, M. Shakeri, M. Riazat and M. Baniassadi, "A new approach to microstructure optimization of solid oxide fuel cell electrodes", *Iranian J. Hydrogen. Fuel. Cell*., Vol. 4, No. 4, pp. 93-102, (2017).

[18] J. Kupecki, "Modelling of Physical, Chemical, and Material Properties of Solid Oxide Fuel Cells", *J. Chem*., Vol. 2015, (2015).

[19] K. Tseronis, I. S. Fragkopoulos, I. Bonis and C. Theodoropoulos, "Detailed Multi-dimensional Modeling of Direct Internal Reforming Solid Oxide Fuel Cells", *Fuel. Cells*., Vol. 16, No. 3, pp. 294–312, (2016).

[20] S. McIntosh and R. J. Gorte, "Direct Hydrocarbon Solid Oxide Fuel Cells".

Chem. Rev, Vol. 104, No. 10, pp. 4845-4865, (2004).

[21] T. Takeguchi, Y. Kani, T. Yano, R. Kikuchi, K. Eguchi, K. Tsujimoto, Y. Uchida, A. Ueno, K. Omoshiki and M. Aizawa, "Study on steam reforming of CH_4 and C_2 hydrocarbons and carbon deposition on Ni-YSZ cermets", *J. Power. Sources.*, Vol. 112, No. 2, pp. 588-595, (2002).

[22] T. Kim, G. Liu, M. Boaro, S. I. Lee, J. M. Vohs, R. J. Gorte, O. H. Al. Madhib and B. O. Dabbousi, "A Study of Carbon Formation and Prevention in Hydrocarbon-Fueled SOFC", *J. Power. Sources*, Vol. 155, No. 2, pp. 231-238, (2006).

[23] A. Mostafaeipour, M. Qolipour, H. Goudarzi, M. Jahangiri, A. M. Golmohammadi, M. Rezaei, A. Goli, L. Sadeghikhorami, A. Sedeh and S. R. Khalifeh, "Implementation of Adaptive Neuro-Fuzzy Inference System (Anfis) for Performance Prediction of Fuel Cell Parameters", *J. Renewable Energy Environ.*, Vol. 6, No. 3, pp. 7-15, (2019).

[24] M. Yan, M. Zeng, Q. Chen and Q. Wang, "Numerical study on carbon deposition of SOFC with unsteady state variation of porosity", *Appl. Energy*, Vol. 97, pp. 754–762, (2012).

[25] H. Xu and Z. Dang. "Lattice Boltzmann modeling of carbon deposition in porous anode of a solid oxide fuel cell with internal reforming", *Appl. Energy.*, Vol. 178, pp. 294–307, (2016).

[26] T. Ma , M. Yan , M. Zeng, J. l. Yuan, Q. Chen, B. Sundén and Q.W. Wang, "Parameter study of transient carbon deposition effect on the performance of a planar solid oxide fuel cell", *Appl. Energy*, Vol. 152, pp. 217-228, (2014).

[27] C. Schluckner, V. Subotic, V. Lawlor and C. Hochenauer, "Carbon Deposition Simulation in Porous SOFC Anodes: A Detailed Numerical Analysis of Major Carbon Precursors", *J. Fuel Cell Sci. Technol*., Vol. 12, No. 5, pp. 1053-1065, (2015).

[28] V. M. Janardhanan and O. Deutschmann, "CFD analysis of a solid oxide fuel cell with internal reforming: Coupled interactions of transport, heterogeneous catalysis and electrochemical processes", *J. Power. Sources.*, Vol. 162, No. 2, pp. 1192-1202, (2006).

[29] H. Pourziaei Araban, J. Alinejad and M. Mohsen Peiravi, "Entropy generation and hybrid fluid-solid-fluid heat transfer in 3D multi-floors enclosure", *Int. J. Exergy.*, Vol. 37, No. 3, pp. 337-357, (2022).

[30] M. M Peiravi and J. Alinejad, "Nano particles distribution characteristics in multi-phase heat transfer between 3D cubical enclosures mounted obstacles", *Alexandria Eng. J.*, Vol. 60, No. 6, pp. 5025-5038, (2021).

[31] M. D. Sanwar, G. Alharbi, K. Z. Islam, and M. d.Islam, "Techno-Economic Analysis of the Hybrid Solar PV/H/Fuel Cell Based Supply Scheme for Green Mobile Communication", *Sustainability*, Vol.13, No. 22, pp.13-22, (2021).

[32] P. Costamagna and K. Honegger, "Modeling at solid oxide heat exchanger integrated stacks and simulation at high fuel utilization", *J. Electrochem. Soc*., Vol. 145, No. 11, pp. 3995-4007, (1998).

[33] M. M. Hussain, X. Li and I. Dincer, "A general electrolyte–electrode-assembly model for the performance characteristics of planar anode-supported solid oxide fuel cells", *J. Power.. Sources*, Vol. 189, No. 2, pp. 916–28, (2009).

[34] O. Razbani, M. Assadi and M. Andersson, "Three dimensional CFD modeling and experimental validation of an electrolyte supported solid oxide fuel cell fed with methane-free biogas", *Int. J. Hydrogen Energy*, Vol. 38, No. 24, pp. 10068-10080, (2013).

[35] H. Iwai, Y. Yamamoto, M. Saito, H. Yoshida, "Numerical simulation of intermediate temperature direct-internal-reforming planar solid oxide fuel cell", *J. Energ*, Vol. 36, No. 4, pp. 2225-2234, (2011).

[36] P. Sarmah, T. K. Gogoi and R. Das, "Estimation of operating parameters of a SOFC integrated combined power cycle using differential evolution based inverse method", *Appl. Therm. Eng*, Vol. 119, pp. 98–107, (2017).

[37] L. Maier, B. Schadel, K. Herrera Delgado, S. Tischer and O. Deutschmann, "Steam Reforming of Methane Over Nickel: Development of a Multi- Step Surface Reaction Mechanism", *Top. Catal.*, Vol. 54, No. 845, pp. 845–858, (2011).

[38] M. Andersson, J. Yuan and B. Sundén, "Modeling Validation and Simulation of an Anode Supported SOFC Including Mass and Heat Transport, Fluid Flow and Chemical Reactions", 9th Int. Conference "*Fuel Cell Science Engineering and Technology"*, Washington, DC, USA, pp. 317-327, (2011).

How to cite this paper:

H. Khoshkam, K. Atashkari and M. Borji, "Unsteady state numerical study of carbon deposition on the performance of solid oxide fuel cell and variation of porosity,", *J. Comput. Appl. Res. Mech. Eng.*, Vol. 12, No. 2, pp. 247-261, (2023).

DOI: 10.22061/JCARME.2022.8347.2124

URL:https://jcarme.sru.ac.ir/?_action=showPDF&article=1787